ANTIOXIDANTS & REDOX SIGNALING
Volume 14, Number 10, 2011

DOI: 10.1089/ars.2010.3468

Inhibition of Na^+/H^+ Exchanger Isoform 1 Is Neuroprotective in Neonatal Hypoxic Ischemic Brain Injury

Pelin Cengiz,[1] Neil Kleman,[2,3] Kutluay Uluc,[2,3] Pinar Kendigelen,[1,4] Tracy Hagemann,[3] Erinc Akture,[1,2] Albee Messing,[3] Peter Ferrazzano,[1,3] and Dandan Sun[2,3]

Abstract

We investigated the role of Na^+/H^+ exchanger isoform 1 (NHE-1) in neonatal hypoxia/ischemia (HI). HI was induced by unilateral ligation of the left common carotid artery in postnatal day 9 (P9) mice, and subsequent exposure of animals to 8% O_2 for 55 min. A pre/posttreatment group received a selective and potent NHE-1 inhibitor HOE 642 (0.5 mg/kg, intraperitoneally) 5 min before HI, then at 24 and 48 h after HI. A posttreatment group received HOE 642 (0.5 mg/kg) at 10 min, 24 h, and 48 h after HI. Saline injections were used as vehicle controls. The vehicle-control brains at 72 h after HI exhibited neuronal degeneration in the ipsilateral hippocampus, striatum, and thalamus, as identified with Fluoro-Jade C positive staining and loss of microtubule-associated protein 2 (MAP2) expression. NHE-1 protein was upregulated in glial fibrillary acidic protein–positive reactive astrocytes. In HOE 642–treated brains, the morphologic hippocampal structures were better preserved and displayed less neurodegeneration and a higher level of MAP2 expression. Motor-learning deficit was detected at 4 weeks of age after HI in the vehicle control group. Inhibition of NHE-1 in P9 mice not only reduced neurodegeneration during the acute stage of HI but also improved the striatum-dependent motor learning and spatial learning at 8 weeks of age after HI. These findings suggest that NHE-1–mediated disruption of ionic homeostasis contributes to striatal and CA1 pyramidal neuronal injury after neonatal HI. *Antioxid. Redox Signal.* 14, 1803–1813.

Introduction

HYPOXIA/ISCHEMIA (HI) is a common cause of brain injury in neonates (6). Molecular mechanisms underlying brain injury in HI are not well defined. Disruption of ionic homeostasis is an important consequence of HI and may contribute to brain injury. Ionic and metabotropic glutamate receptor–mediated overload of intracellular Na^+ and Ca^{2+} is well documented in the literature (12, 22, 36). However, it remains unexplored whether non–glutamate-mediated mechanisms are involved in Na^+ and H^+ ionic dysregulation and hippocampal injury after HI. Most important, brain intracellular alkalosis was recently shown to correlate with the severity of brain injury in term infants with neonatal HI (27). The infants with the most-alkaline brain pH_i demonstrated more-severe brain injury in the first 2 weeks after birth and worse neurodevelopmental outcome at 1 year of age (27). This persistent brain intracellular alkalosis is thought to result from excessive activation of the Na^+/H^+ exchanger (NHE).

NHE is a membrane protein that regulates intracellular pH (pH_i) by extrusion of 1 H^+ in exchange for 1 Na^+ (23). Thus, acidosis after HI may trigger excessive activation of NHE and lead to intracellular Na^+ overload and secondary ischemic brain injury. The NHE isoform 1 (NHE-1) is the most abundant isoform in rat brains among nine NHE isoforms (18). Pharmacologic inhibition of NHE-1 activity attenuates the detrimental consequences of ischemia and reperfusion injury in myocardium and focal cerebral ischemia in adult animal studies (1, 19). Administration of the nonselective NHE inhibitor *N*-methyl-isobutyl-amiloride (MIA) ameliorates neonatal brain injury in a mouse HI model (13). Pretreatment of adult gerbils with the amiloride derivative ethylisopropylamiloride (EIPA), a nonselective NHE inhibitor, significantly reduces the extent of CA1 pyramidal neuronal loss after global ischemia (9). These studies suggest that NHE activation is involved in neuronal injury after HI.

In the current study, we investigated whether inhibition of NHE-1 with the potent inhibitor HOE 642 is neuroprotective after HI in immature brains. We report here that the HOE 642–treated brains displayed better-preserved morphology in the hippocampus, accompanied by less neurodegeneration and a

Departments of [1]Pediatrics and [2]Neurological Surgery, University of Wisconsin School of Medicine and Public Health, and [3]Waisman Center, Madison, Wisconsin.
[4]Department of Anesthesiology, Istanbul University Cerrahpaşa Medical School, Istanbul,Turkey.

higher level of MAP2 expression. HOE 642 treatment improved the long-term neurologic function after HI.

Materials and Methods

Materials

Fluoro-Jade C (FJ-C) was from Histo-Chem Inc. (Jefferson, AK). Tissue-Tek O.C.T. compound was from Sakura Finetek (Torrance, CA). Antibodies against microtubule-associated protein 2 (MAP2) and glial fibrillary acidic protein (GFAP) were from Sigma (St. Louis, MO) and Dako Inc. (Carpinteria, CA), respectively. Polyclonal NHE-1 antibody was from Abcam Inc. (Cambridge, MA). HOE 642 was a kind gift from Aventis Pharma (Frankfurt, Germany). Goat anti-mouse Alexa Fluor 488-conjugated IgG and goat anti-rabbit Alexa Fluor 546-conjugated IgG were from Invitrogen (Carlsbad, CA). Tissue section–rinsing solution CitriSolv was from Fisher Inc. (Hampton, NH), and DPX mounting medium was from Sigma Inc.

Induction of neonatal HI

Postnatal day 9 (P9) C57BL/6J mice were anesthetized with isofluorane (4% for induction, 1% for maintenance), 30% O_2, and 70% N_2. The body temperature of the animal was maintained at 37°C with a heating pad. Under a surgical microscope, a midline skin incision (0.5 cm) was made on the neck, and the left common carotid artery was exposed and electrically cauterized. The incision was rinsed with 1% lidocaine and sutured with a 6.0 polypropylene (Prolene) suture. Animals were returned to their dams and observed continuously for 30 min during a 2-h recovery period. To induce ipsilateral ischemic injury as described by Vannucci *et al.* (33), the animals were placed in a hypoxia chamber (BioSpherix Ltd, Redfield, NY), equilibrated with 8% O_2, 92% N_2 at 37°C, for 55 min. After HI, animals were monitored continuously for 30 min and then checked every 30 min for 2 h and then daily until sacrificed.

Drug administration

To inhibit selectively NHE-1 with its potent inhibitor HOE 642, the animals were randomly divided into four treatment groups: pre/posttreated, posttreated, and the corresponding two vehicle (saline) controls. The pre/posttreated group received the initial dose of HOE 642 (0.5 mg/kg) 10 min before HI and subsequently at 24 and 48 h after HI, intraperitoneal (IP). The posttreated group received a dose of 0.5 mg/kg HOE 642 (IP) at 10 min and 24 and 48 h after HI. HOE 642 was administered at multiple time points because the intravenous half-life of HOE 642 is short (40 min in rats) (29). The two vehicle control groups received an equal volume of saline at the same time points.

Brain-tissue preparation

At 72 h after HI, animals were anesthetized with isoflurane, as described earlier. Animals were transcardially perfused with 4% paraformaldehyde and decapitated. After postfixation of the brains in 4% paraformaldehyde overnight, brains were stored in a 30% sucrose/PBS solution for 48 h and sectioned (35 or 70 μm thickness) on a freezing sliding microtome (Leica SM2000R, Leica, Bannockburn, IL). The brain sections were either cryoprotected in an antifreeze solution for storage at −20°C or mounted on polylysine-coated slides.

FJ-C staining and Quantification

Mounted brain sections (70 μm) were dried on a slide warmer at 50°C for 30 min. The following steps were performed in the dark. Sections were treated with 0.06 % $KMnO_4$ for 15 min. After a brief rinse in ddH_2O, the sections were stained with 0.001% FJ-C in 1% acetic acid for 25 min on a shaker. Sections were rinsed 3×1 min in ddH_2O, and followed by air-drying on the slide warmer at 50°C for 8 min. Slides were then rinsed in CitriSolv and mounted with DPX mounting medium. FJ-C–stained images were taken by using a Nikon TE300 epifluorescence microscope equipped with an FITC filter. In a blind manner, the total number of FJ-C–positive cells in the ipsilateral CA1 region of hippocampus was determined in each slice by using Metamorph image-analysis software (Molecular Devices, Downington, PA). The entire CA1 region of two brain sections (210 μm apart) per brain, 10 to 13 brains/group, was analyzed. To create whole-brain images, a mosaic was obtained by using an epifluorescence microscope (Zeiss Axioplan 2, 2.5×objective lens) equipped with a motorized stage and compiled with Stereo-Investigator software (MBF Biosciences, Williston, VT).

Double immunofluorescence staining

After rinsing with Tris-buffered saline (TBS), brain sections (35 μm) were incubated with TBS^{++}(0.1% Triton X-100 and 3% goat serum in 0.1 *M* TBS) for 30 min at 37°C. Sections were double-stained with a monoclonal antibody against MAP2 (1:500), rabbit polyclonal antibody against GFAP (1:500), or polyclonal anti-NHE-1 antibody (1:100) for 1 h at 37°C and then overnight at 4°C. After washing with TBS (3×10 min), brain sections were incubated for 1 h at 37°C with goat anti-mouse Alexa Fluor 488-conjugated IgG (for MAP2, 1:200) and goat anti-rabbit Alexa Fluor 546-conjugated IgG (for GFAP, 1:200). After rinsing with TBS, sections were incubated in To-Pro-3 Iodide (1:1,000 in TBS^{++}) for 15 min and mounted on slides. Slides were imaged with a Leica DMIRE 2 inverted confocal microscope and Leica microscope software (Leica Inc.).

Immunoblotting

To investigate expression of NHE-1 during development, whole-brain tissues were harvested from P1, P3, P5, P7, P9, P12, P15, and P30 mice. Brain tissues were homogenized and centrifuged at 2,200 *g* for 3 min at 4°C. The pellet was suspended and centrifuged again. To obtain the crude membrane proteins, the combined supernatants were centrifuged at 12,200 *g* for 8 min at 4°C. The protein content was determined by the bicinchionic acid method (Pierce, Rockford, IL). The protein samples (150 μg) and prestained molecular-mass markers in a SDS buffer were electrophoretically separated on 10% SDS gels. The resolved proteins were electrophoretically transferred to a nitrocellulose membrane. After incubation in 7.5% nonfat dry milk in TBS for 1 h, the blots were probed with the anti-NHE-1 antibody (1:1,000) overnight at 4°C. After rinsing with TBS, the blots were incubated with goat anti-rabbit horseradish peroxidase-conjugated secondary IgG (1:2,000) for 1 h. Bound antibodies were visualized by using the enhanced chemiluminescence assay.

Quantification of GFAP with ELISA

GFAP was quantified with ELISA, as previously described (7). Brain tissues were dissected on ice to collect cortical cortex (posterior to bregma, including subcortical white matter), striatum, hippocampus, and cerebellum. Tissues were homogenized (~50 mg/ml) in 2% SDS; 50 m*M* Tris-HCl pH 7.4; 5 m*M* EDTA; 1 m*M* PefablocSC supplemented with Complete Protease Inhibitor Cocktail (Roche Applied Sciences, Indianapolis, IN), and boiled for 15 min. Protein concentrations were quantified with the bicinchionic acid assay. ELISA was performed in microtiter plates coated with monoclonal anti-GFAP cocktail SMI-26 (1:1,000 in PBS; Covance, Princeton, NJ) and blocked with BLOTTO (5% milk in PBS). Protein samples were diluted in PBS with 0.5% TritonX-100/1% BSA, and 0.1 to 5 ng analyzed per well. Serial dilutions of purified GFAP (Research Diagnostics, Inc., Flanders, NJ) were used as standards. Polyclonal anti-GFAP was used for the detection antibody (DAKO, Carpinteria, CA) at 200 ng/ml in BLOTTO-TX (0.5% TritonX-100). Peroxidase-conjugated goat anti-rabbit IgG antibody (Sigma) was used for the secondary antibody (1:10,000 in BLOTTO-TX). Wells were rinsed with PBS (before addition of protein samples) or PBS/0.5% TritonX-100 (after incubation with protein samples) between all incubations. The presence of peroxidase activity was detected with the addition of SuperSignal ELISA Femto Maximum Sensitivity Substrate (Pierce Biotechnology, Rockford, IL) and quantified with a GloRunner Microplate Luminometer (Turner Biosystems, Sunnyvale, CA).

Locomotor activity in the open field

Behavioral testing was conducted by a single researcher who was blinded to the treatment groups (sham control, vehicle HI control, or the HOE 642 posttreatment after 55 min HI). The locomotor test was performed when the mice reached 4 weeks of age. An open-field test was conducted in a room (378×317 cm) painted white and illuminated by overhead fluorescent lights. The open-field arena was a square white Plexiglass box (55×55×20 cm), with a digital camera attached to a National Instruments video capture board mounted directly above the open-field arena. The open-field arena was divided virtually into 16 equal squares, via a 4×4 grid, to assist in data analysis. Video and data were recorded by using Coulbourn Instruments LimeLight2 software (Whitehall, PA) configured to capture four images per second (sec). Path data (x and y coordinates of tracked mouse) were exported into a spreadsheet for analyses. Animals were transported from the housing room and allowed to acclimate to the room for 30 min before testing. Sessions lasted 30 min, and each mouse was evaluated once. Sessions began with the removal of an individual mouse from its home cage and placement in the center of the arena. The distance traveled in 30 min was measured to reflect locomotor activity.

Accelerating Rotarod test

The accelerating Rotarod test examines balance and motor coordination as well as skill learning. The accelerating Rotarod test was performed when the mice reached 4 weeks of age. After mice were placed onto a horizontal rotating rod at 4 rpm (model ENV-575M; Med Associates, St. Alban, CT), Rotarod was accelerated from 4 to 40 rpm over the course of a 5min trial. A single test lasted from the time the mouse was placed on the rotating rod until it fell off or until 5 min had elapsed. If a mouse grasped the wheel and made one complete revolution, the latency to the first complete revolution was recorded (21). The mouse was then returned to the home cage. Mice were tested for four trials per day for 3 consecutive days (14). Average time on the rotating rod across days was presented. The mice rested in their home cages for 20 min to 1 h between each trial.

Hidden Morris Water Maze test

Spatial learning was assessed with the Morris Water Maze test, which was conducted when mice reached 8 weeks of age. Mice were trained to locate a hidden escape platform in a circular pool full of water. The pool had an inside diameter of 124 cm (136 cm outside) and was 45 cm tall. The clear acrylic hidden escape platform was 30 cm tall, with a circular top, 10 cm in diameter. A Panasonic Digital CCTV (model WV-BP334) camera was mounted to the ceiling, directly above the pool. Video was acquired with a Piccolo Diligent video capture board and analyzed with Noldus Instruments EthoVison XT software. The room was 441×332 cm in size and illuminated by overhead fluorescent lights. The walls were painted white with distal visual cues hung on each wall (with a background noise of 56 dB). The pool was filled with 31 cm of water (21–23° C), and illumination at the water level was 21 lux. White, nontoxic paint was added until the water was opaque (about 550 g of Crayola Nontoxic liquid paint). Thus, the platform was hidden by 1 cm of colored water. Last, the pool was virtually divided into equal quadrants with four virtual points, west, north, east, and south. The escape platform was placed in the center of the NW quadrant, 26 cm from the wall at the 45-degree diagonal from center.

Mice were transported from the housing room to the testing room. Mice were allowed to acclimate to the room for 30 min before training or testing. A brief preliminary training was conducted with each mouse to ensure that it could swim and climb onto the platform. Each mouse was trained for eight trials (two blocks) per day for 4 days (a total of 32 trials). Between each trial, mice were allowed to rest on the platform for 10 to 15 sec. Trials lasted 1 min or until the mouse found the platform. If the mouse did not find the platform, the mouse was placed on the platform for 10 to 15 s by the researcher. Latency to reach the platform was automatically tracked and recorded. After trial 32, each animal was given a probe trial, during which the platform was removed, and each animal was allowed 60 s to search for the platform in the pool. The amount of time that each animal spent in the trained quadrant and the other quadrants was recorded.

Visible Platform (Cued) Morris Water Maze test

To rule out a possibility of visual impairment in animals after HI, a follow-up study was conducted by using a visible platform in the Morris Water Maze test. The procedure was nearly identical to the standard hidden-platform version of the test. The cued platform had a cube-shaped box on the platform that protrudes above the water surface. Each mouse received 2 blocks (4 trials per block) per day for 2 consecutive days. Trials lasted 60 s or until the mouse found the platform. The platform was moved to a new, random location in every trial. All trials were from a different start location. If the mouse

found the escape platform, it was allowed to rest for 10 s on the platform. If the mouse did not find the platform, it was gently guided to the platform and allowed to survey the surroundings for 10 s. At least 1 h elapsed between consecutive blocks.

Statistical analysis

Values are expressed as the mean ± SD except for Fig. 5 (mean ± SEM). Statistical analysis was performed by using the Mann–Whitney rank sum test to compare vehicle control and the drug-treated group. ANOVA (the Bonferroni post test) was used in the case of multiple comparisons (SigmaStat; Systat Software, Point Richmond, CA). For behavioral testing, repeated-measures analysis of variance was performed. The p values smaller ≤ 0.05 were considered statistically significant.

Results

Inhibition of NHE-1 with HOE 642 reduces neuronal injury in hippocampus, striatum, and thalamus

To investigate whether NHE-1 activity plays a role in neuronal injury after HI, the effect of the potent NHE-1 inhibitor HOE 642 was examined. Brain injury was assessed with FJ-C staining, a method that detects degenerative cells (28). As shown in Fig. 1A, hippocampal injury was visible in the ipsilateral hemisphere of the vehicle control animal, as reflected by hippocampal atrophy (arrowhead in the brightfield image).

FJ-C–positive cells were detected in the ipsilateral hippocampus in CA1, CA2, and CA3 regions, as well as in the thalamus (Fig. 1B, arrowhead). In contrast, in the animals treated before and after with HOE 642, the ipsilateral hippocampus exhibited smaller lesions, reflected by better preserved hippocampal morphology (Fig. 1C, arrow) and fewer FJ-C–positive cells in the pyramidal neuronal layers of CA1, CA2, and CA3 (Fig. 1D, arrow). In the posttreatment vehicle control animals, FJ-C–positive cells appeared in ipsilateral hippocampus, striatum, thalamus, and some cerebral cortical areas (Fig. 1F, arrowhead). The animals posttreated with HOE 642 after HI exhibited neuroprotection in these brain regions, with no FJ-C–positive cells visible in the ipsilateral striatum and thalamus, and fewer FJ-C–positive cells found in pyramidal neuronal layers of CA2 and CA3 (Fig. 1H). These data clearly illustrate the neuroprotective effects of inhibiting NHE-1 activity with HOE 642 after HI.

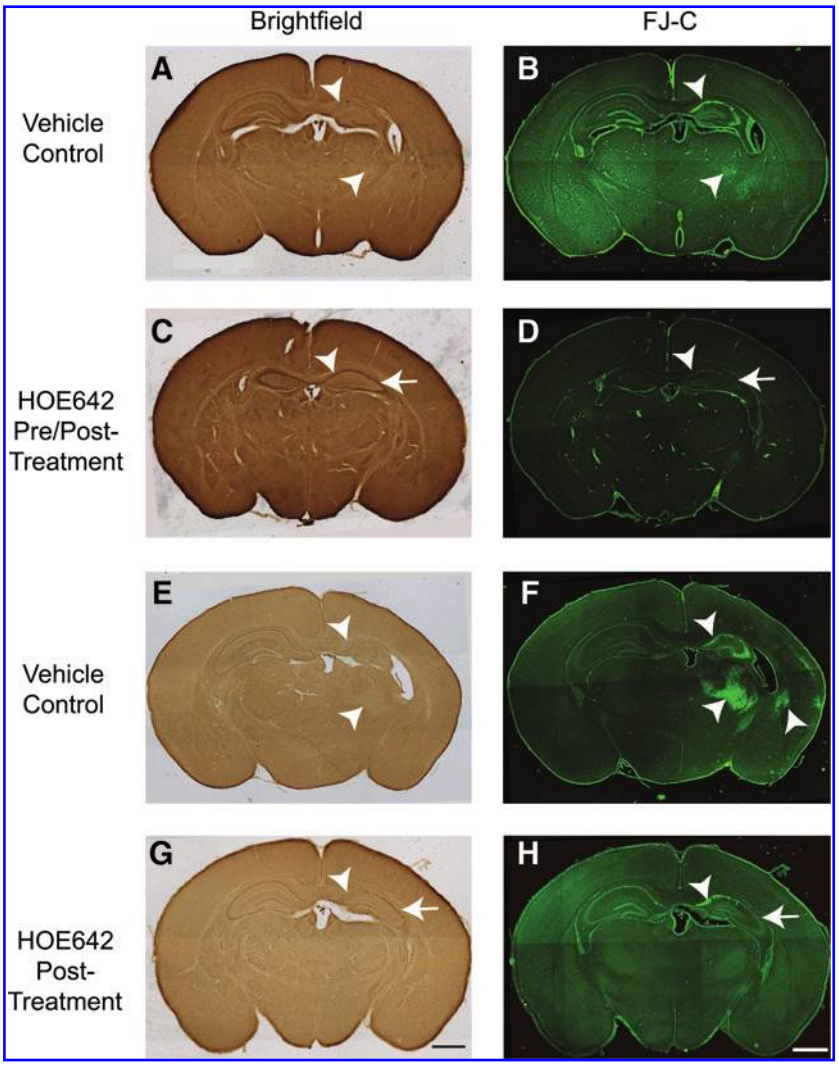

FIG. 1. Inhibition of NHE-1 with HOE 642 reduces neuronal damage in hippocampus and striatum. FJ-C staining was performed to assess neuronal damage in the ipsilateral hippocampus and striatum at 72 h after HI. **(A, C, E, G)** Brightfield images. **(B, D, F, H)** FJ-C staining. **(A, B, E, F)** Vehicle (saline) controls. **(C, D)** Pre posttreatment with the initial dose of HOE 642 (0.5 mg/kg, IP) administered at 5 min before HI induction, and three subsequent doses (0.5 mg/kg, IP) administered at 24 h and 48 h after HI. **(G, H)** Posttreatment with HOE 642 (0.5 mg/kg, IP) administered at 10 min, 24 h, and 48 h after HI. Multiple doses were used to maintain an effective drug concentration [half-life of HOE 642, 40 min in rats (29)]. *Arrowhead,* Severe degeneration. *Arrow,* reduced cell degeneration. Scale bar, 1 mm. (To see this illustration in color the reader is referred to the web version of this article at www.liebertonline.com/ars).

Quantitative analysis of neuroprotection mediated by HOE 642 in CA1 regions

As shown in Fig. 2A (a), background, a nonspecific signal of FJ-C staining was detected in the contralateral hippocampus of P9 brain at 72 h after HI (arrow). In contrast, the ipsilateral hippocampus exhibited a higher level of specific FJ-C fluorescence signals in CA1, CA2, CA3, and DG regions [Fig. 2A (b), arrowhead]. Fig. 2A (c) illustrates the magnified ipsilateral hippocampal image with a clearly increased number of FJ-C–positive cells in the CA1 pyramidal neuronal layers (arrowhead). The HOE 642 pre/posttreated brains showed fewer FJ-C–positive cells [Fig. 2A (d), arrow].

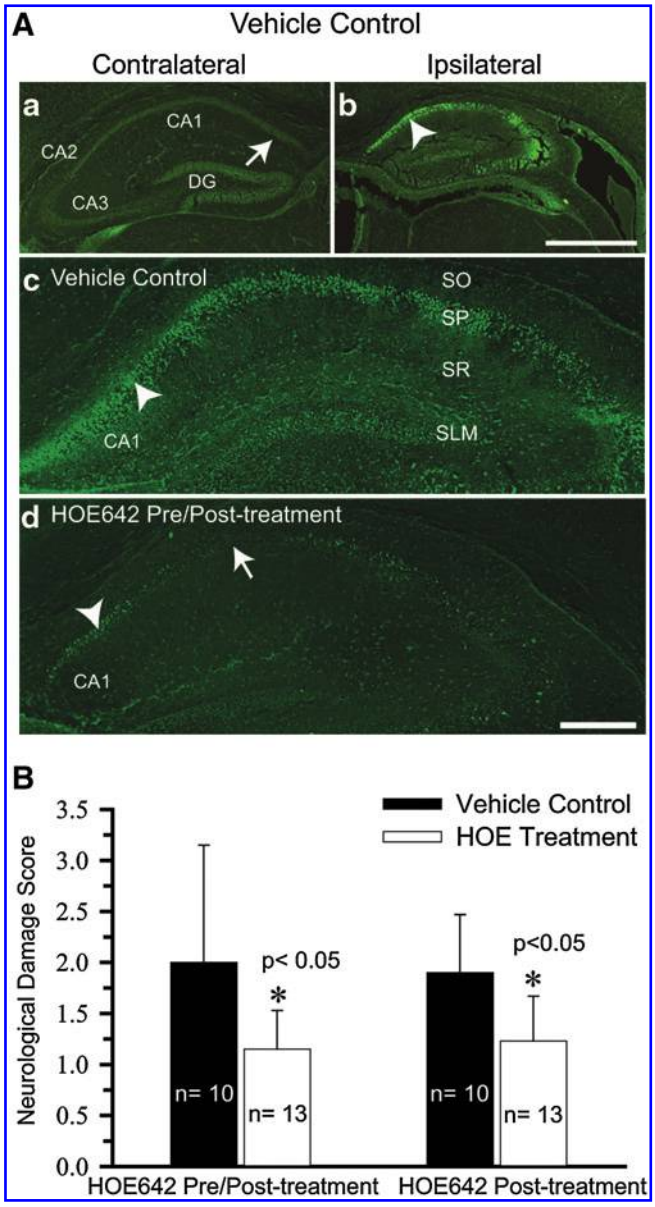

FIG. 2. Quantification of HOE 642–mediated protection in CA1 hippocampal neurons. (A) Brain sections were harvested at 72 h after 55-min HI and stained with FJ-C. **(a, b)** FJ-staining images of the contralateral and ipsilateral hippocampus in the vehicle control mouse. **(c, d)** Magnified images of CA1 region of the ipsilateral hippocampus in vehicle control or HOE 642 pre/posttreated mouse. *Arrowhead,* Severe degeneration. *Arrow,* reduced degeneration. Specific hippocampal regions are indicated as SO, stratum oriens; SP, stratum pyramidale; SR, stratum radiatum; SLM, stratum lacunosum. Scale bar, 1 mm **(a, b)** and 100 μm **(c, d)**. **(B)** Data are expressed as mean neurologic damage score $\pm$ SD. A score was given as the following: 0, no FJ-C–positive cells; 1, 1–500; 2, 501–1,000; 3, 1,001–1,500; 4, >1,500 FJ-C–positive cells. (To see this illustration in color the reader is referred to the web version of this article at www.liebertonline.com/ars).

The CA1 pyramidal neuronal injury was quantified by counting the number of FJ-C–positive cells in the vehicle control and in animals treated with HOE 642. Based on the number of FJ-C–positive cells, a score was assigned: 0, no FJ-C–positive cells; 1, 1–500; 2, 501–1,000; 3, 1,001–1,500; 4, >1,500 FJ-C–positive cells. As shown in Fig. 2B, both HOE 642 treatment groups (pre/post- and posttreated) exhibited statistically significant reductions of FJ-C–positive cells in the ipsilateral CA1 region of the hippocampus ($p < 0.05$).

Inhibition of NHE-1 activity by HOE 642 attenuated loss of MAP2 expression after HI

We also investigated hippocampal neuronal injury by examining changes of MAP2 expression. MAP2 is a dendritic protein thought to be involved in microtubule assembly, which is an essential step in neurogenesis. The contralateral hippocampus of the vehicle control mice exhibited abundant MAP2 expression [Fig. 3A (a)]. The hippocampal regions, such as stratum pyramidale (SP) and stratum radiatum (SR), show the well-organized structure of the cell body and dendrites [Fig. 3A (c), arrow]. The 55-min HI caused an apparent loss of pyramidal neurons and MAP2, accompanied by organization of the SR in the ipsilateral hippocampus [Fig. 3A (b)]. These changes were more clearly illustrated in the magnified image [Fig. 3A (d)]. In mice pre/posttreated with HOE 642, the loss of MAP2 expression after HI was attenuated in the ipsilateral hippocampus [Fig. 3A (f)]. Structural organization of dendrites was preserved in the stratum radiatum of the ipsilateral hippocampus of the HOE 642 pre/posttreated brains [Fig. 3A (h), arrow].

NHE-1 is expressed exclusively in GFAP-positive ($GFAP^+$) reactive astrocytes in ipsilateral hippocampus after HI

Reactive astrocytes were detected by $GFAP^+$ staining in the ipsilateral hippocampus after HI. In the vehicle control brain after HI, a few $GFAP^+$ cells were located in the contralateral stratum oriens (SO), SR, stratum lacunosum, and moleculare (SLM) of the hippocampus [Fig. 3A (c), open arrowhead]. However, the ipsilateral hippocampus showed an increased number of $GFAP^+$ cells in the SO, SP, SR, and SLM of the CA1 region [Fig. 3A (b, d)]. Inhibition of NHE-1 activity with HOE 642 did not alter the number of reactive astrocytes, despite its effect on preservation of CA1 neurons and expression of MAP2 in dendrites [Fig. 3A (f, h)]. This finding was further confirmed by quantification of GFAP expression with ELISA. As shown in Fig. 3B, at 72 h after HI, a low level of GFAP expression was detected in the contralateral hippocampus, striatum, cortex, and cerebellum. Striatum and cortex exhibited a lower GFAP expression than that in the hippocampus and cerebellum ($\sim$16–29 vs. $\sim$258–294 ng/mg protein). These values were not different from those of the sham controls ($p > 0.05$). In contrast, the GFAP level was increased by

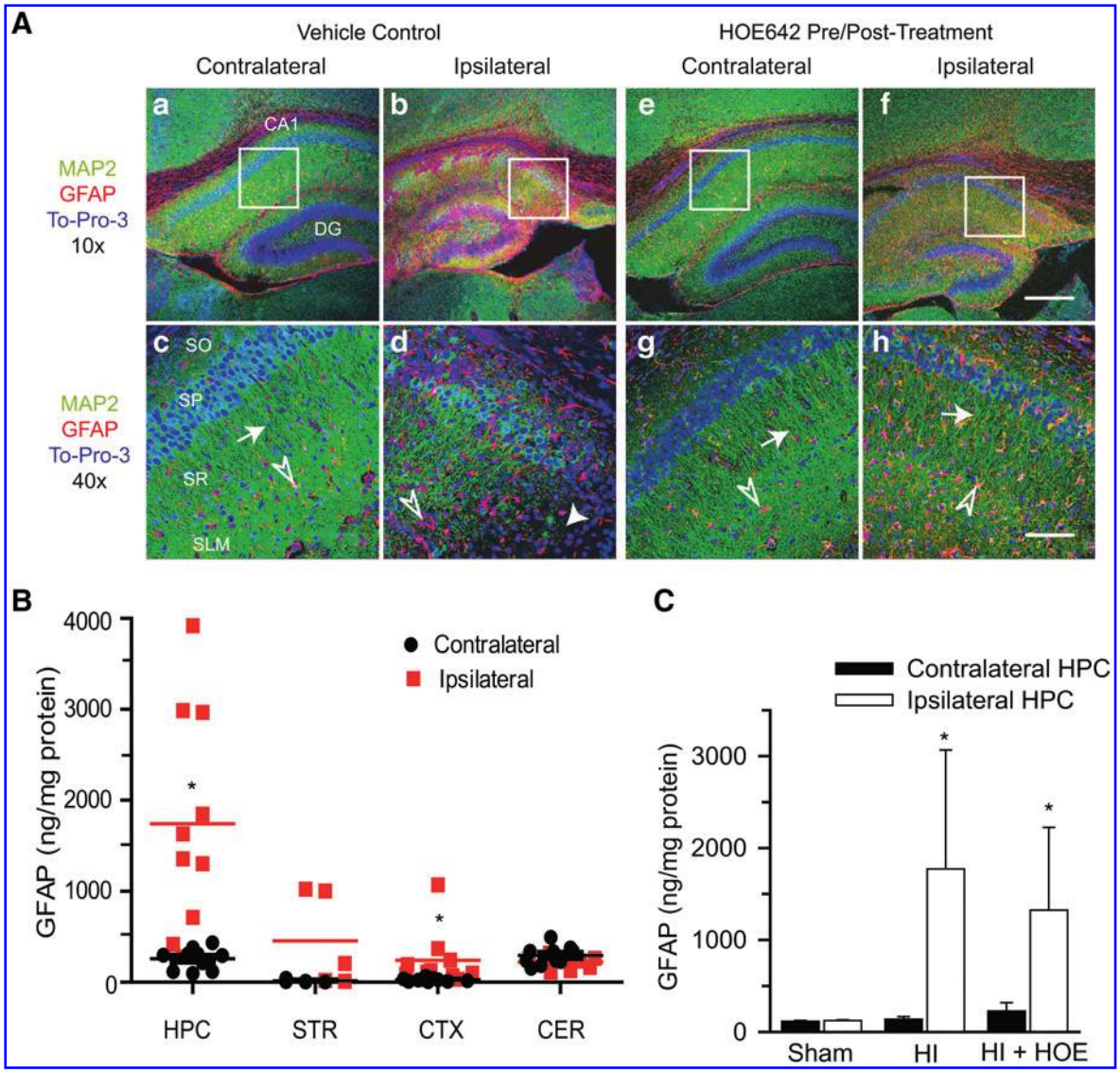

FIG. 3. Changes of MAP2 in the ipsilateral hippocampus after HI. (A) Changes of MAP2 and GFAP in the ipsilateral hippocampus were examined at 72 h after HI. The vehicle control and HOE 642 pre/posttreatment are described in the Fig. 1 legend. Specific hippocampal regions (SO, SP, SR, SLM) were indicated similar to the Fig. 2 legend. **(a, b, e, f)** Double immunostaining for MAP2 (green) and GFAP (red) in the CA1 regions. ToPro-3 Iodide (blue) was used as a nuclear stain. **(c, d, g, h)** The 40×magnification of the CA1 region is indicated in the white boxes. *Arrowhead*, Severe degeneration. *Arrow*, Reduced degeneration. *Open arrowhead*, $GAFP^{+}$–reactive astrocytes. Scale bar, 300 μm **(a, b, e, f)** and 75 μm **(c, d, g, h)**. Images were representative of $n = 8$ in each group. **(B)** GFAP content was measured in hippocampus (HPC), striatum (STR), cortex (CTX), and cerebellum (CER) at 72 h after HI. **(C)** GFAP content in hippocampi (HPC) of Sham control ($n = 3$), HI (n = 10), or HI + HOE 642 (posttreatment group, $n = 7$) mice at 72 h. Data are expressed as mean ± SD. *$p < 0.05$ vs. contralateral. (To see this illustration in color the reader is referred to the web version of this article at www.liebertonline.com/ars).

~6.5-fold in the ipsilateral hippocampus and ~8.5-fold in the ipsilateral cortex ($p < 0.05$). A tendency was noted toward elevated levels of GFAP protein in the ipsilateral striatum, but not reaching statistical significance ($p = 0.06$). Moreover, inhibition of NHE-1 with HOE 642 did not affect the elevation of GFAP immunoreactivity in hippocampus after HI (Fig. 3C). This finding was consistent with the GFAP immunostaining data.

NHE-1 expression of hippocampus after HI

Next, we evaluated the expression of NHE-1 protein. A developmental-dependent elevation of NHE-1 expression was noted in immature brains. A low level of NHE-1 was detected in P1 brain and increased in the P5-P12 brains. P12-P30 brain tissues exhibited a sustained level of NHE-1 expression. The β-tubulin III protein loading controls were similar among these samples (Fig. 4A).

Changes of NHE-1 expression in hippocampus after HI were further characterized by immunofluorescence staining. The contralateral CA1 pyramidal layers in the vehicle control and animals treated with HOE 642 exhibited a low level of NHE-1 expression at 72 h after HI [green, Fig. 4B (a, c), arrow]. The immunoreactive signals for NHE-1 were specific because they were absent when the NHE-1 primary antibody

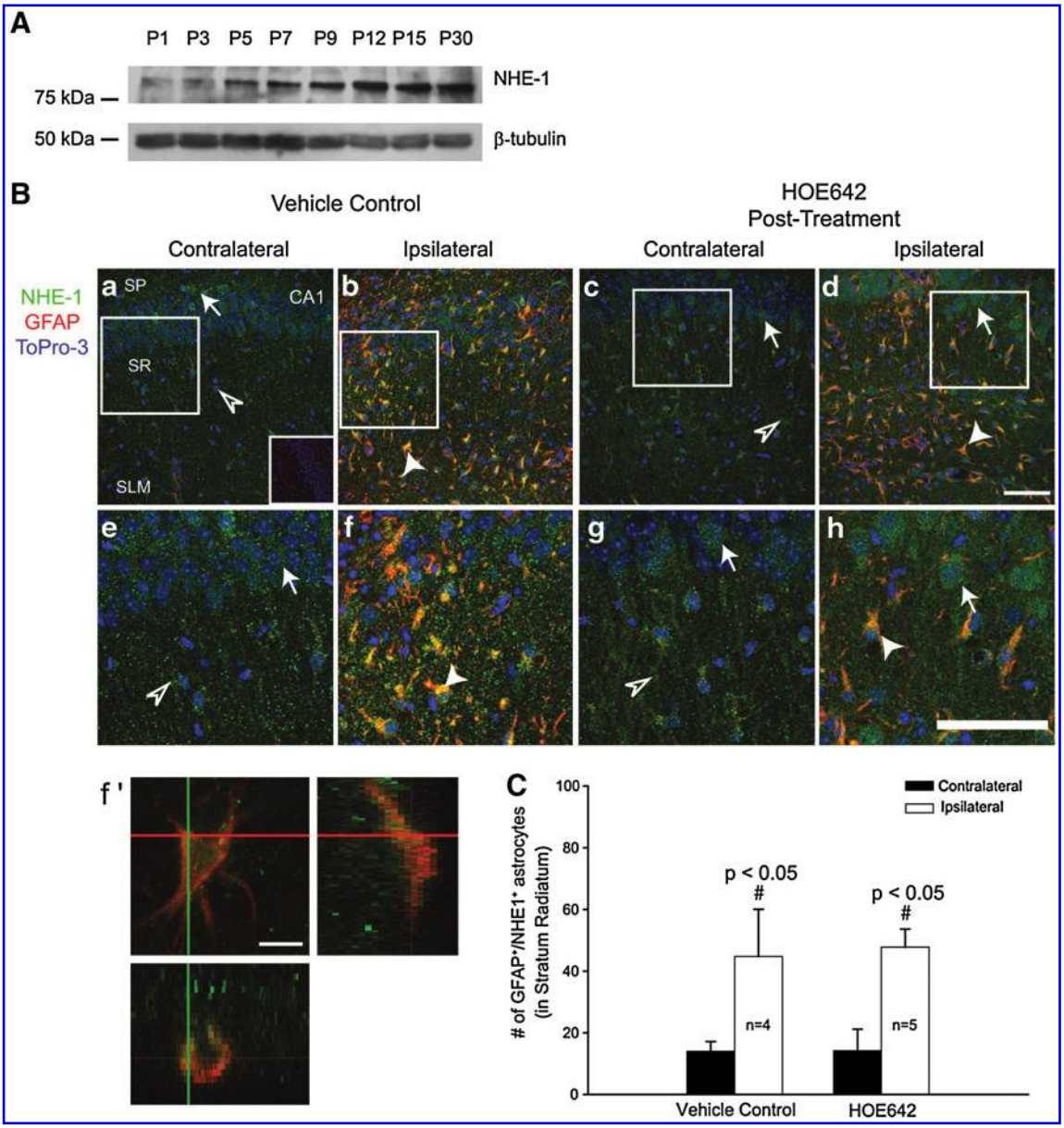

FIG. 4. Changes of NHE-1 expression in the hippocampus after HI. (A) Expression of NHE-1 was determined in P1-P30 mouse brains. Total protein (150 μg) was loaded per lane, and the immunoblot was probed for NHE-1 and β-tubulin on the same blot. **(B)** Immunofluorescence staining in the CA1 region of brains at 72 h after HI: NHE-1 (red), GFAP (green), and To-Pro-3 (blue). Specific hippocampal regions (SP, SR, SLM) were indicated similar to the Fig. 2 legend. **(a, b)** Vehicle control brain. **(c, d)** HOE 642 posttreated brain. **(e–h)** Magnified regions indicate the box in **(a–d). (f′)** z-Section image in **(f)**. **(C)** Summary data. Data are expressed as mean ± SD; $n = 4$–5. *Arrowhead,* NHE-1/GFAP double-positive cells. Scale bar, 75 μm (a–d, e–h) and 10 μm (in f′). *Arrow,* **CA1** neuron*; open arrowhead,* nonreactive astrocytes lacking GFAP expression. (To see this illustration in color the reader is referred to the web version of this article at www.liebertonline.com/ars).

was omitted [inset in Fig. 4B (a)]. Of interest, many cells in the contralateral SR and SLM were positive for the NHE-1 immunoreactivity [Fig. 4B (a, c), open arrowhead] unlike the $GFAP^+$ astrocytes. These cells may represent nonreactive astrocytes. In the ipsilateral hippocampus of the vehicle control brain, the CA1 SP layer was disorganized. The striking change in the SR and SLM was an increase in number of cells that had both GFAP and NHE-1 immunoreactivity [Fig. 4B (b), arrowhead]. These changes are clearly illustrated in the magnified images [Fig. 4B (e, f)]. The z-section analysis showed that the $NHE\text{-}1^+/GFAP^+$ cells exhibited reactive astrocyte morphology with enlarged processes and hypertrophy of the cell body [Fig. 4B (f)]. Interestingly, NHE-1 was upregulated in the CA1 pyramidal neurons in the in the brains of animals treated with HOE 642 [Fig. 4B (d)]. Treatment of animals after HI with HOE 642 did not attenuate formation of the $GFAP^+$ astrocytes in every layer of the ipsilateral hippocampus [Fig. 4B (d, h)]. Summary data shown in Fig. 4C indicate that NHE-1 is abundantly expressed in the reactive astrocytes. NHE-1 may play an important role in reactive astrogliosis, which may be contributing to neuronal damage.

Locomotor activity and motor function in mice after HI

To examine whether inhibition of NHE-1 activity during the acute HI has long-lasting effects on neuronal function, we first evaluated motor function and learning in the vehicle control and in animals treated with HOE 642 at 4 weeks of age after HI. As shown in Fig. 5A, exploratory locomotion in the open field showed that naive control and sham animals traveled similar distance ($3{,}005 \pm 106$ cm/30 min and $3{,}141 \pm 205$ cm/30 min, respectively). Animals in the HI vehicle control group traveled slightly farther ($3{,}928 \pm 463$ cm/30 min), but it was not significantly different ($p > 0.05$). Moreover, the mice treated with HOE 642 showed similar locomotor activity ($2{,}558 \pm 530$ cm/30 min). These data imply that brain injury mediated by HI does not significantly affect locomotor activity and motor function in mice. This view is further supported by the normal motor activity of HI animals in trial 1 in the Accelerating Rotarod test (Fig. 5B).

Corticostriatal circuits are involved in motor learning in the accelerating Rotarod task, which examines striatum-dependent motor learning (4). In light of the striatal injury in the ipsilateral hemisphere after HI, we investigated whether motor-learning ability in the Accelerating Rotarod test was different in the vehicle control and in mice treated with HOE 642. The time on the Accelerating Rotarod during trial 1 was similar among four groups at 4 weeks of age after HI (Fig. 5B). This suggests that HI does not impair motor coordination and balance in the vehicle control and HOE 642–treated mice. However, sham animals and animals treated with HOE 642 showed clearly improved motor learning on days 2 and 3 (Fig. 5C; $p < 0.05$). In contrast, vehicle controls did not demonstrate any change in performance between day 1 and days 2 and 3 (Fig. 5C).

We further investigated spatial learning by using the hidden Morris Water Maze test. Fig. 5D shows that sham animals exhibited significantly less platform latency time in the hidden Morris Water Maze test on days 2–4. HI animals demonstrated spatial learning by day 4, whereas the HOE 642–treated group shortened the platform latency time on days 3 and 4. The visible platform (cued) Morris Water Maze

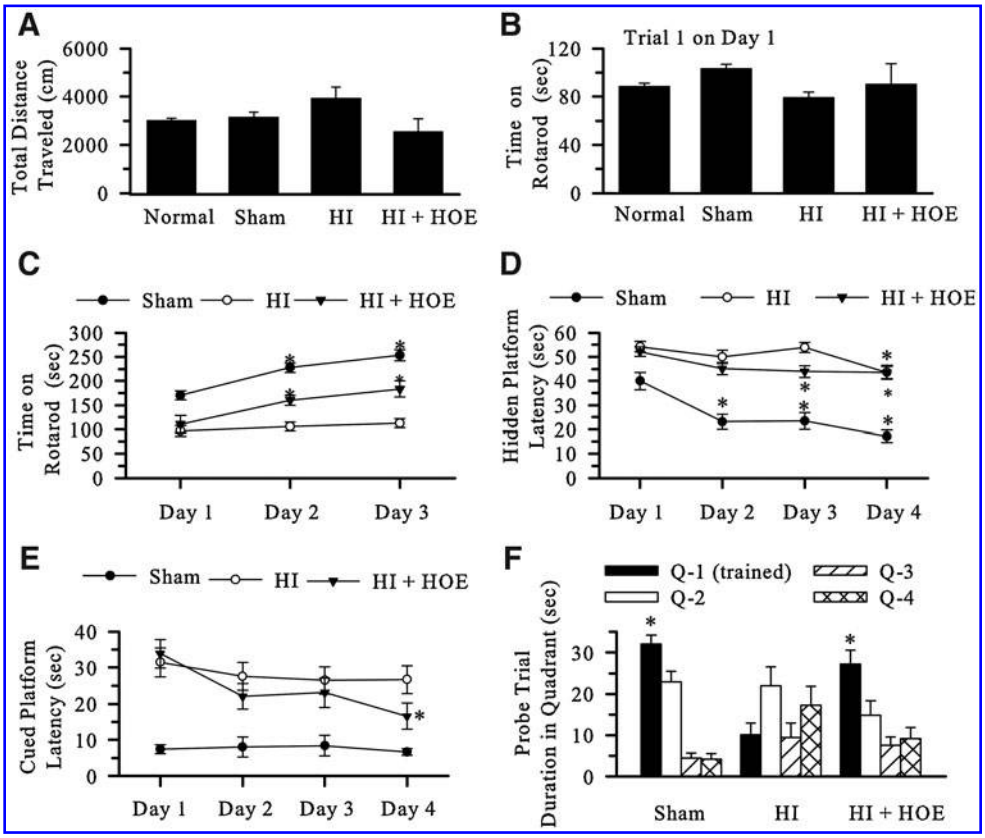

FIG. 5. Inhibition of NHE-1 P9 improved the long-term neuronal function. (A) Locomotor activity in the open field. Normal control, Sham control, vehicle control (HI), and animals treated with HOE 642 (HI+HOE) were tested for open-field activity at 4 weeks of age after HI. Data are expressed as mean ± SEM for total distance traveled in 30 min ($n = 5$–12). **(B)** The Accelerating Rotarod motor-learning test. Time spent in the first trial on the first day at 4 weeks of age after HI. Data are expressed as mean ± SEM ($n = 6$–19). **(C)** The Accelerating Rotarod motor-learning test. The average time spent on the Rotarod for four trials per day for 3 consecutive days at 4 weeks of age after HI. Data are expressed as mean ± SEM ($n = 6$–19). *$p < 0.05$ vs. day 1 in each group. **(D)** Hidden Morris Water Maze test. The platform latency on the hidden Water Maze was analyzed in Sham, HI, and HI+HOE groups at 8 weeks of age after HI. Data are expressed as mean ± SEM ($n = 5$–10). *$p < 0.05$ vs. day 1 in each group. **(E)** Visible (Cued) platform Morris Water Maze test. The visible platform latency was analyzed in sham, HI, and HI+HOE groups at 8 weeks of age after HI. Data are expressed as mean ± SEM ($n = 5$–10). **(F)** Hidden Morris Water Maze test probe trial. Time spent in each quadrant was analyzed in Sham, HI, and HI+HOE groups at 8 weeks of age after HI. Data are expressed as mean ± SEM ($n = 5$–10). *$p < 0.05$ vs. quadrant 1 (Q-1; training quadrant) in each group.

test illustrated that visual acuity in all groups was similar (Fig. 5E). Moreover, Fig. 5F shows that time spent in the training quadrant in sham and HOE 642–treated animals was significantly greater than that in the other quadrants in the probe trial. In contrast, vehicle control animals spent similar time in each quadrant. This further suggests that spatial learning in HOE 642–treated animals was better than that in the vehicle controls.

Discussion

Expression of NHE-1 in hippocampus

NHE-1 is expressed in virtually all cells and tissues and is, by far, the most abundant plasma membrane NHE isoform in the rat brain (18). An *in situ* hybridization analysis showed that NHE-1 mRNA appears at higher levels in the hippocampus, compared with NHE-2, NHE-3, and NHE-4 (18). Expression of NHE-1 in rat brains is dependent on the state of development and peaks on day of life 13 (5). We also detected an upregulation of NHE-1 in mouse brains from P1 to P12, which was sustained between P12 and 30.

In the current study, we found that NHE-1 was expressed in hippocampal pyramidal neurons and astrocytes throughout the hippocampus. Most important, NHE-1 immunostaining was enhanced in both CA1 neurons and reactive astrocytes at 72 h after HI. The z-section analysis with the confocal microscopy confirmed the colocalization of GFAP and NHE-1. These findings are consistent with the recent report showing the elevation of NHE-1 expression in reactive astrocytes in CA1 regions of adult gerbil brains after a transient global ischemia (9). Taken together, these studies imply that hippocampal neurons and astrocytes may respond to the intracellular acidosis after HI by upregulating NHE-1 expression and function. Alternately, we cannot rule out the possibility that some of the NHE-1 immunoreactive signals in the ipsilateral hippocampus may be localized in microglia. Expression of NHE-1 has been detected in Iba 1–positive cells after global ischemia (9).

Inhibition of NHE-1 with HOE 642 is neuroprotective in neonatal brains after HI

Many reports have shown that NHE inhibition with nonselective inhibitors is neuroprotective against ischemic hippocampal injury. Pretreatment of adult gerbils with the amiloride derivative 5-(*N*-ethyl-*N*-isopropyl)-amiloride (EIPA), a nonselective NHE inhibitor, significantly reduced the extent of CA1 pyramidal neuronal loss at 6 days after global ischemia (26). Pretreatment of P7 mice with the nonspecific NHE inhibitor MIA at 30 min before the induction of HI increased the forebrain tissue survival from 44% to 67% (13). In the case in which the brain injury was localized to the hippocampus with a mild HI, inhibition of NHE with MIA significantly reduced the injury score and TUNEL-positive cells (13). These reports suggest that NHE plays a role in HI. However, the mechanism of neuroprotection mediated by NHE-1 after HI remains unknown.

In the current study, we examined the effects of selective NHE-1 inhibition with its potent inhibitor HOE 642 on hippocampal injury after HI. HOE 642 is a potent and highly selective NHE-1 inhibitor [IC_{50} for NHE-1 is 0.01 μM; NHE-2, 1.6 μM; NHE-3, 1,000 μM (23)]. The selectivity of HOE 642 on blocking NHE-1 has been established in parallel studies using HOE 642 in NHE-$1^{+/+}$ neurons, NHE-$1^{+/+}$ astrocytes, and NHE-$1^{-/-}$ neurons or astrocytes (16, 17). HOE 642 selectively inhibits NHE-1–mediated H^+ extrusion in the NHE-$1^{+/+}$ cells but has no effects in NHE-$1^{-/-}$ neurons or NHE-$1^{-/-}$ astrocytes. Therefore, the neuroprotective benefit with the HOE 642 treatment in this study can most likely be attributed to inhibition of NHE-1.

Our two HOE 642 treatment groups (pre/post-, and post-HI treatment) clearly demonstrate the efficacy of pharmacologic blockade of NHE-1, evident with the decreased neurodegeneration of striatal pyramidal neurons and CA1 neurons and preservation of MAP2 expression and hippocampal organization. The mice treated with HOE 642 after HI also exhibited improved motor learning at 4 weeks of age after HI. This is likely due to reduced injury in the striatum and hippocampus, because the HOE 642–treated brains rarely exhibited FJ-C–positive degenerative cells in the ipsilateral striatum. The corticostriatal circuits play an important role in slow and fast motor-skill learning in mice (4), and the motor learning in the Accelerating Rotarod task represents striatum-dependent learning (10, 14). Therefore, the HOE 642–mediated neuroprotection in striatum is important for long-term functional recovery after HI.

Moreover, our current study detected deficits in the hippocampus-dependent spatial navigation in the HI animals. Both bilateral dorsal hippocampal lesions in adult animals and unilateral neonatal HI injury can cause similar degrees of performance deficit on the spatially oriented tasks like the hidden water maze (32). It has been reported that the degree of structural and behavioral abnormalities in the hippocampus correlates with the duration of HI [45-, 60-, and 75-min hypoxia, (20)], with the 65–70% in 75-min HI animals exhibiting performance deficit in spatial navigation versus 20–34% in animals with 45-min HI. In the probe trial, we observed that the time spent in the training quadrant was longer in the HOE 642–treated animals, compared with the vehicle controls. This finding suggests that HOE 642 treatment not only decreases the hippocampal pyramidal neuronal injury but also improves the spatial learning after neonatal HI.

Neuroprotective mechanisms by inhibiting NHE-1

Maintaining the pH_i values close to neutrality is a crucial task for a wide variety of cells. It is generally accepted that low pH_i values influence neuronal excitability and inhibit synaptic transmission (3, 35). NHE constitutes the most efficient means of eliminating excessive acid from actively metabolizing cells (23). Activation of NHE activity in hippocampal nerve terminals has been detected after intracellular acidification under normoxic conditions (11, 31). This elevated NHE activity is accompanied by an increase in $[Na^+]_i$ and $[Ca^{2+}]_i$ as well as increased postsynaptic currents (11, 31). The authors attribute these changes to concurrent activation of NHE and the reverse mode of Na^+/Ca^{2+} exchange in the nerve terminals, which leads to Ca^{2+}-mediated excessive release of neurotransmitters.

Robertson *et al.* (27) reported a relation between brain intracellular alkalosis and the severity of brain injury in term infants with neonatal encephalopathy (27). In the current study, we speculate that NHE-1 activity is overstimulated after HI as a result of protein upregulation or posttranslational

regulation. HOE 642 may protect CA1 neurons by reducing NHE-1 and Na^+/Ca^{2+} exchanger–mediated intracellular Na^+ and Ca^{2+} overload and mitochondrial dysfunction in CA1 neurons. This view is further supported by our recent report that stimulation of NHE-1 in cultured cortical neurons caused dendritic Na^+_i accumulation, swelling, and a concurrent loss of Ca^{2+}_i homeostasis and mitochondrial bioenergetics after oxygen and glucose deprivation (15). It has been suggested that the second wave of injury after 48 h after HI is mediated largely by apoptosis (22). In the current study, HOE 642–mediated reduction of FJ-C–positive cells at 72 h after HI may reflect a decrease in apoptotic cell death in CA1 pyramidal neurons.

Abundant expression of NHE-1 in reactive astrocytes

Hippocampal astrocytes exhibit an extremely intimate relation with neurons, which is characterized by a single hippocampal astrocyte contacting several hundred dendrites from multiple neurons and enveloping hundreds of thousands of synapses (30). Thus, astrocytes play a direct role in hippocampal neuronal function by maintaining ionic and neurotransmitter homeostasis of the synaptic interstitial fluid. Astrocytes can alter neuronal excitability through changing astrocyte Ca^{2+} or by regulating release of synaptically active "gliotransmitters" (glutamate, ATP, and adenosine) (8, 25).

Hippocampal astrocytes respond to HI by developing reactive astrogliosis, which is reflected by upregulation of GFAP expression, astrocyte hypertrophy, and proliferation (9, 24, 34). In the current study, we detected a sharp elevation in GFAP expression in reactive astrocytes of the CA1 regions after HI, which was accompanied by hypertrophy. Interestingly, NHE-1 and GFAP were colocalized in the SR, SO regions of the ipsilateral hippocampus at 72 h after HI. Surprisingly, we did not find the decrease in NHE-1/GFAP double-stained cells or attenuation of the HI-induced GFAP upregulation in the HOE 642–treated brains, despite the reduced CA1 neuronal injury. This leads us to speculate that NHE-1 activity in reactive astrocytes may be detrimental to neuronal survival. HOE 642 may offer neuroprotection in part through inhibition of NHE-1 activity in reactive astrocytes, indirectly protecting hippocampal neurons by reducing the detrimental effects of reactive astrocytes. This interpretation is supported by a recent report that NHE activity in hippocampal astrocytes is indeed stimulated after hypoxia (2). Currently, it is not clear how blocking NHE-1 activity in reactive astrocytes can reduce neuronal injury in the hippocampus after HI. We hypothesize that this may result from reducing NHE-1–mediated Na^+ influx and astrocyte swelling, which can increase the driving force for Na^+-dependent glutamate transporter and promote glutamate uptake from the synaptic interstitial fluid. The decrease in NHE-1 and Na^+/Ca^{2+} exchange may also prevent Ca^{2+} elevation in reactive astrocytes and reduce gliotransmitter release and proinflammatory cytokine release.

In the current study, we investigated a role for NHE-1 in hippocampal injury after HI by pharmacologically blocking NHE-1 activity with its potent inhibitor HOE 642. The vehicle control HI brains exhibited neuronal degeneration in the ipsilateral striatum, thalamus, and CA1 pyramidal neurons at 72 h. HI also triggered moderate astrogliosis in the ipsilateral hippocampus. Interestingly, the $GFAP^+$-reactive astrocytes expressed an abundant level of NHE-1. Pharmacologic inhibition of NHE-1 activity reduced neurodegeneration in striatum, thalamus, and hippocampus and improved striatum-dependent motor learning. These findings suggest that NHE-1–mediated disruption of ionic homeostasis can contribute to CA1 pyramidal neuronal injury after neonatal HI. The HOE 642 posttreatment results indicate the potential of targeting NHE-1 in the development of more-effective therapies for HI in neonates.

Acknowledgments

We thank Douglas Kintner and Margaret Griesemer for technical assistance.

Author Disclosure Statement

This work was supported in part by University of Wisconsin Department of Pediatrics Research & Development Grant (P.C.), 1UL1RR025011 from the Clinical and Translational Science Award program of NCRR and NIH (P.F.), AHA SURF 09UFEL2260340 (N.K.), NIH grants RO1NS38118 and RO1NS48216 and AHA EIA 0540154 (D.S.), NIH grants RO1NS42803 and RO1NS060120 (A.M.), and NIH P30 HD03352 (Waisman Center).

References

1. Avkiran M. Protection of the ischaemic myocardium by Na^+/H^+ exchange inhibitors: potential mechanisms of action. *Basic Res Cardiol* 96: 306–311, 2001.
2. Bevensee MO and Boron WF. Effects of acute hypoxia on intracellular-pH regulation in astrocytes cultured from rat hippocampus. *Brain Res* 1193: 143–152, 2008.
3. Chesler M. Regulation and modulation of pH in the brain. *Physiol Rev* 83: 1183–1221, 2003.
4. Costa RM, Cohen D, and Nicolelis MA. Differential corticostriatal plasticity during fast and slow motor skill learning in mice. *Curr Biol* 14: 1124–1134, 2004.
5. Douglas RM, Schmitt BM, Xia Y, Bevensee MO, Biemesderfer D, Boron WF, and Haddad GG. Sodium-hydrogen exchangers and sodium-bicarbonate co-transporters: ontogeny of protein expression in the rat brain. *Neuroscience* 102: 217–228, 2001.
6. Ferriero DM. Neonatal brain injury. *N Engl J Med* 351: 1985–1995, 2004.
7. Hagemann TL, Connor JX, and Messing A. Alexander disease-associated glial fibrillary acidic protein mutations in mice induce Rosenthal fiber formation and a white matter stress response. *J Neurosci* 26: 11162–11173, 2006.
8. Halassa MM, Fellin T, and Haydon PG. The tripartite synapse: roles for gliotransmission in health and disease. *Trends Mol Med* 13: 54–63, 2007.
9. Hwang IK, Yoo KY, An SJ, Li H, Lee CH, Choi JH, Lee JY, Lee BH, Kim YM, Kwon YG, and Won MH. Late expression of Na^+/H^+ exchanger 1 (NHE1) and neuroprotective effects of NHE inhibitor in the gerbil hippocampal CA1 region induced by transient ischemia. *Exp Neurol* 212: 314–323, 2008.
10. Iwai M, Stetler RA, Xing J, Hu X, Gao Y, Zhang W, Chen J, and Cao G. Enhanced oligodendrogenesis and recovery of neurological function by erythropoietin after neonatal hypoxic/ischemic brain injury. *Stroke* 41: 1032–1037, 2010.
11. Jang IS, Brodwick MS, Wang ZM, Jeong HJ, Choi BJ, and Akaike N. The Na(+)/H(+) exchanger is a major pH regulator in GABAergic presynaptic nerve terminals synapsing

onto rat CA3 pyramidal neurons. *J Neurochem* 99: 1224–1236, 2006.
12. Jiang X, Mu D, Biran V, Faustino J, Chang S, Rincon CM, Sheldon RA, and Ferriero DM. Activated Src kinases interact with the *N*-methyl-D-aspartate receptor after neonatal brain ischemia. *Ann Neurol* 63: 632–641, 2008.
13. Kendall GS, Robertson NJ, Iwata O, Peebles D, and Raivich G. *N*-methyl-isobutyl-amiloride ameliorates brain injury when commenced before hypoxia ischemia in neonatal mice. *Pediatr Res* 59: 227–231, 2006.
14. Kheirbek MA, Britt JP, Beeler JA, Ishikawa Y, McGehee DS, and Zhuang X. Adenylyl cyclase type 5 contributes to corticostriatal plasticity and striatum-dependent learning. *J Neurosci* 29: 12115–12124, 2009.
15. Kintner DB, Chen X, Currie J, Chanana V, Ferrazzano P, Chiu SY, Baba A, Matsuda/ T, Cohen MS, Orlowski J, Taunton J, and Sun D. Excessive Na^+/H^+ exchange in disruption of dendritic Na^+ and Ca^{2+} homeostasis and mitochondrial dysfunction following *in vitro* ischemia. *J Biol Chem* 2010, in press.
16. Kintner DB, Su G, Lenart B, Ballard AJ, Meyer JW, Ng LL, Shull GE, and Sun D. Increased tolerance to oxygen and glucose deprivation in astrocytes from Na^+/H^+ exchanger isoform 1 null mice. *Am J Physiol Cell Physiol* 287: C12–C21, 2004.
17. Luo J, Chen H, Kintner DB, Shull GE, and Sun D. Decreased neuronal death in Na^+/H^+ exchanger isoform 1-null mice after in vitro and in vivo ischemia. *J Neurosci* 25: 11256–11268, 2005.
18. Ma E and Haddad GG. Expression and localization of Na^+/H^+ exchangers in rat central nervous system. *Neuroscience* 79: 591–603, 1997.
19. Masereel B, Pochet L, and Laeckmann D. An overview of inhibitors of Na(+)/H(+) exchanger. *Eur J Med Chem* 38: 547–554, 2003.
20. McAuliffe JJ, Miles L, and Vorhees CV. Adult neurological function following neonatal hypoxia-ischemia in a mouse model of the term neonate: water maze performance is dependent on separable cognitive and motor components. *Brain Res* 1118: 208–221, 2006.
21. McIlwain KL, Merriweather MY, Yuva-Paylor LA, and Paylor R. The use of behavioral test batteries: effects of training history. *Physiol Behav* 73: 705–717, 2001.
22. Northington FJ, Ferriero DM, Graham EM, Traystman RJ, and Martin LJ. Early neurodegeneration after hypoxia-ischemia in neonatal rat is necrosis while delayed neuronal death is apoptosis. *Neurobiol Dis* 8: 207–219, 2001.
23. Orlowski J and Grinstein S. Na^+/H^+ exchangers of mammalian cells. *J Biol Chem* 272: 22373–22376, 1997.
24. Ouyang YB, Voloboueva LA, Xu LJ, and Giffard RG. Selective dysfunction of hippocampal CA1 astrocytes contributes to delayed neuronal damage after transient forebrain ischemia. *J Neurosci* 27: 4253–4260, 2007.
25. Perea G, Navarrete M, and Araque A. Tripartite synapses: astrocytes process and control synaptic information. *Trends Neurosci* 32: 421–431, 2009.
26. Phillis JW, Estevez AY, Guyot LL, and O'Regan MH. 5-(*N*-Ethyl-*N*-isopropyl)-amiloride, an Na^+-H^+ exchange inhibitor, protects gerbil hippocampal neurons from ischemic injury. *Brain Res* 839: 199–202, 1999.
27. Robertson NJ, Cowan FM, Cox IJ, and Edwards AD. Brain alkaline intracellular pH after neonatal encephalopathy. *Ann Neurol* 52: 732–742, 2002.
28. Schmued LC, Stowers CC, Scallet AC, and Xu L. Fluoro-Jade C results in ultra high resolution and contrast labeling of degenerating neurons. *Brain Res* 1035: 24–31, 2005.
29. Scholz W, Albus U, Counillon L, Gogelein H, Lang HJ, Linz W, Weichert A, and Scholkens BA. Protective effects of HOE-642, a selective sodium-hydrogen exchange subtype 1 inhibitor, on cardiac ischaemia and reperfusion. *Cardiovasc Res* 29: 260–268, 1995.
30. Sofroniew MV and Vinters HV. Astrocytes: biology and pathology. *Acta Neuropathol* 119: 7–35, 2010.
31. Trudeau LE, Parpura V, and Haydon PG. Activation of neurotransmitter release in hippocampal nerve terminals during recovery from intracellular acidification. *J Neurophysiol* 81: 2627–2635, 1999.
32. van Praag H, Qu PM, Elliott RC, Wu H, Dreyfus CF, and Black IB. Unilateral hippocampal lesions in newborn and adult rats: effects on spatial memory and BDNF gene expression. *Behav Brain Res* 92: 21–30, 1998.
33. Vannucci RC and Vannucci SJ. Perinatal hypoxic-ischemic brain damage: evolution of an animal model. *Dev Neurosci* 27: 81–86, 2005.
34. Xiong M, Yang Y, Chen GQ, and Zhou WH. Post-ischemic hypothermia for 24 h in P7 rats rescues hippocampal neuron: association with decreased astrocyte activation and inflammatory cytokine expression. *Brain Res Bull* 79: 351–357, 2009.
35. Xiong ZQ, Saggau P, and Stringer JL. Activity-dependent intracellular acidification correlates with the duration of seizure activity. *J Neurosci* 20: 1290–1296, 2000.
36. Zhou M, Xu W, Liao G, Bi X, and Baudry M. Neuroprotection against neonatal hypoxia/ischemia-induced cerebral cell death by prevention of calpain-mediated mGluR1alpha truncation. *Exp Neurol* 218: 75–82, 2009.

Address correspondence to:
Pelin Cengiz, M.D.
Department of Pediatrics
University of Wisconsin-Madison
School of Medicine and Public Health
Box 4108, Clinical Sciences Center-H4/464
600 Highland Ave.
Madison, WI 53792

E-mail: cengiz@pediatrics.wisc.edu

Date of first submission to ARS Central, July 11, 2010; date of final revised submission, August 1, 2010; date of acceptance, August 13, 2010.

Abbreviations Used

CA (1,2,3) = *cornu Ammonis*
DG = dentate gyrus
GFAP = glial fibrillary acidic protein
HI = hypoxia/ischemia
MAP2 = microtubule-associated protein 2
NHE = Na^+/H^+ exchanger
NHE-1 = Na^+/H^+ exchanger isoform 1
SLM = stratum lacunosum moleculare
SO = stratum oriens
SP = stratum pyramidale
SR = stratum radiatum

This article has been cited by:

1. Yejie Shi, Vishal Chanana, Jyoti J. Watters, Peter Ferrazzano, Dandan Sun. 2011. Role of sodium/hydrogen exchanger isoform 1 in microglial activation and proinflammatory responses in ischemic brains. *Journal of Neurochemistry* no-no. [CrossRef]
2. Pelin Cengiz, Kutluay Uluc, Pinar Kendigelen, Erinc Akture, Elizabeth Hutchinson, Chihwa Song, Louise Zhang, Jihae Lee, Greg E. Budoff, Elizabeth Meyerand, Dandan Sun, Peter Ferrazzano. 2011. Chronic Neurological Deficits in Mice after Perinatal Hypoxia and Ischemia Correlate with Hemispheric Tissue Loss and White Matter Injury Detected by MRI. *Developmental Neuroscience* **33**:3-4, 270-279. [CrossRef]